RESEARCH ARTICLE

National Science Review
8: nwaa179, 2021
doi: 10.1093/nsr/nwaa179
Advance access publication 25 August 2020

MOLECULAR BIOLOGY & GENETICS

A single-cell transcriptome atlas of the aging human and macaque retina

Wenyang Yi[1,†], Yufeng Lu[2,6,†], Suijuan Zhong[3,8,†], Mei Zhang[1,4,*,†], Le Sun[2,6], Hao Dong[2,6], Mengdi Wang[2], Min Wei[1], Haohuan Xie[1], Hongqiang Qu[9], Rongmei Peng[9], Jing Hong[9], Ziqin Yao[1], Yunyun Tong[1], Wei Wang[2,6], Qiang Ma[2,6], Zeyuan Liu[2,6], Yuqian Ma[1], Shouzhen Li[1], Chonghai Yin[2], Jianwei Liu[2], Chao Ma[10], Xiaoqun Wang[2,5,6,7,11,12,*], Qian Wu[3,8,*] and Tian Xue[1,4,5,11,*]

[1]Eye Center at The First Affiliated Hospital of USTC, Hefei National Laboratory for Physical Sciences at the Microscale, School of Life Sciences, Division of Life Sciences and Medicine, University of Science and Technology of China, Hefei 230026, China; [2]State Key Laboratory of Brain and Cognitive Science, Institute of Brain-Intelligence Technology (Shanghai), Bioland Laboratory (Guangzhou), Institute of Biophysics, Chinese Academy of Sciences, Beijing 100101, China; [3]State Key Laboratory of Cognitive Neuroscience and Learning, Beijing Normal University, Beijing 100875, China; [4]Neurodegenerative Disorder Research Center, CAS Key Laboratory of Brain Function and Disease, University of Science and Technology of China, Hefei 230026, China; [5]Institute for Stem Cell and Regeneration, Chinese Academy of Sciences, Beijing 100101, China;

(Continued on next page)

*Corresponding authors. E-mails: xuetian@ustc.edu.cn; qianwu@bnu.edu.cn; xiaoqunwang@ibp.ac.cn; zhangmei@ustc.edu.cn
†Equally contributed to this work.

Received 24 May 2020; **Revised** 9 July 2020; **Accepted** 24 July 2020

ABSTRACT

The human retina is a complex neural tissue that detects light and sends visual information to the brain. However, the molecular and cellular processes that underlie aging primate retina remain unclear. Here, we provide a comprehensive transcriptomic atlas based on 119 520 single cells of the foveal and peripheral retina of humans and macaques covering different ages. The molecular features of retinal cells differed between the two species, suggesting distinct regional and species specializations of the human and macaque retinae. In addition, human retinal aging occurred in a region- and cell-type-specific manner. Aging of human retina exhibited a foveal to peripheral gradient. *MYO9A*$^{-}$ rods and a horizontal cell subtype were greatly reduced in aging retina, indicating their vulnerability to aging. Moreover, we generated a dataset showing the cell-type- and region-specific gene expression associated with 55 types of human retinal disease, which provides a foundation to understanding of the molecular and cellular mechanisms underlying human retinal diseases. Such datasets are valuable to understanding of the molecular characteristics of primate retina, as well as molecular regulation of aging progression and related diseases.

Keywords: single-cell RNA sequencing, primate retina, aging, cell heterogeneity, age-related disease, cell-cell communication

INTRODUCTION

The human retina is a specialized light-sensitive tissue of neurons, glia and nourishing blood vessels [1–3]. The retina has long served as a model system for developmental and functional studies of the central nervous system [4,5]. Different cell types in the retina, including rod and cone photoreceptors as well as bipolar (BCs), amacrine (ACs), horizontal (HCs), ganglion (GCs) and glial cells, are packed together into a tightly organized network that converts incoming light into electrochemical signals, which are then relayed to the brain for visual formation [1]. In addition to this complexity, primates, including humans and monkeys, possess a specialized fovea, which is absent in rodent models. The fovea, which is responsible for high-acuity vision, is enriched in cone photoreceptors that directly receive light and are supported by specific morphological Müller glia (MGs) [6]. The molecular differences between the foveal and peripheral retina are important for understanding human visual function. To date, multiple analyses in primates have demonstrated the region-specific retinal transcriptomes in developing and adult foveal and peripheral retina, suggesting distinct transcriptional regulations in the two regions [3,7–12].

As people age, a deterioration in photoreceptor structure occurs in the human retina, particularly in the foveal region. Patients aged ≥60 years display obvious reductions in the number of foveal photoreceptors, and a decline in color discrimination and vision sensitivity [13]. Moreover, they are at

high risk for retinal diseases, such as age-related macular degeneration (AMD). To date, however, key information on the molecular changes in aging human retina at single-cell resolution is lacking. In particular, it is unclear whether different cell types in the human foveal and peripheral retina exhibit distinct molecular changes during aging. Incomplete understanding of the aging process and underlying complexities has restricted development of therapeutic strategies to slow or reverse retinal aging, which could otherwise help to postpone or rescue age-related retinal diseases.

Nonhuman primate (NHP) models have been widely used to study human retinal development and visual function [14,15]. Although human and macaque retina share many similarities, such as genetics, anatomy, physiology and immunology, there are also differences between them. For example, at birth, the monkey fovea appears to have more mature cone morphology than that of human, whereas the human fovea develops rapidly during infancy [16]. In addition, the cone subtype ratios are different across the two species [17]. So far, detailed molecular and cellular signatures between the different cell types in human and macaque retina remain elusive. In particular, whether various cell types in the human and macaque retina exhibit different molecular changes following aging is largely unknown.

As the primate retina is a heterogeneous tissue containing various cell types, the transcriptional heterogeneity of retinal cells cannot be detected using conventional bulk RNA-sequencing (RNA-seq). In contrast, single cell RNA-sequencing (scRNA-seq) has the power to detect region- and cell-type-specific changes, especially for rare cell types. In addition, scRNA-seq can decipher ligand-receptor crosstalk between cell-cell interactions [18]. To decipher the detailed molecular processes that accompany retinal aging, we mapped >119,000 cell transcriptomes of the human and macaque (*Macaca mulatta*) retina from young to old stages and explored related gene transcriptional regulation using scRNA-seq and the bulk Assay for Transposase-Accessible Chromatin with high-throughput sequencing (bulk ATAC-seq). Our data revealed that although the human and macaque retina showed high similarity in major cell types, the molecular features were distinguishable between species. Rods showed the greatest interspecies variation. Although rods from humans and macaques could be divided into two subtypes by *MYO9A* expression, the proportion of subtypes varied between the species. Interestingly, MGs and cones not only exhibited regional transcription differences, they also interacted with each other by ligand-receptor regulation. Furthermore, aging in the human foveal retina occurred earlier than that of the peripheral retina, and *MYO9A*$^{-}$ rods and one HC subtype showed greater vulnerability to aging. Finally, we generated a dataset showing the cell-type- and region-specific gene expression associated with 55 types of human retinal disease. Overall, our study provides a valuable data source for understanding the regional and species specializations of the human and macaque retina as well as the molecular regulation of aging progression and related diseases.

RESULTS

Single-cell transcriptomes of primate retina

We collected single-cell transcriptomic profiles of 119,520 cells, including 38,558 from six healthy human samples (one 8-day-old infant and, five adults aged between 35 and 87 years) and 80,962 from five macaque samples (one 2-year-old juvenile and four adults aged between 4 and 23 years) (Supplementary Table 1), which covered progressive retinal aging, using droplet-based scRNA-seq (10x Genomics platform). Retinae were dissociated from 1.5–2.0 mm and 5 mm diameter pieces around the center of the foveal pit to represent foveal and peripheral cells, respectively (Fig. 1a–c, Supplementary Fig. 1a). In total, cell atlases of 45,231 foveal and 74,289 peripheral cells were collected. The sequencing depth was analyzed by the gene number per cell in each sample (Supplementary Fig. 1b). We performed unbiased clustering of cell profiles from the human retina with both foveal and peripheral regions and found 56 clusters (Supplementary Fig. 1c). Cells from the 8-day-old infant generally clustered together and differed from cells from other samples. As human photoreceptors do not reach maturation until 4 years old [19], the cells in the 8-day-old infant were not as mature as those of the adults (Supplementary Fig. 1c). Interestingly, some clusters showed regional specificity, e.g. Clusters 13, 22 and 51 showed foveal identity and Clusters 21, 32 and 43 showed peripheral identity (Supplementary Fig. 1c). With known cell-type markers, we grouped 56 clusters into 11 major classes, including six neuronal cell types (rods, cones, HCs, ACs, BCs and GCs), three glial cell types (MGs, astrocytes and microglia), endothelial cells and pericytes (Fig. 1b, Supplementary Fig. 1d and e, Supplementary Table 2). Interestingly, we found that cells from Human-Clusters 46 and 51 (which were rod and MG subgroups,

(Continued from previous page)

[6]University of Chinese Academy of Sciences, Beijing 100049, China; [7]Advanced Innovation Center for Human Brain Protection, Beijing Institute for Brain Disorders, Capital Medical University, Beijing 100069, China; [8]IDG/McGovern Institute for Brain Research, Beijing Normal University, Beijing 100875, China; [9]Department of Ophthalmology, Beijing Key Laboratory of Restoration of Damaged Ocular Nerve, Peking University Third Hospital, Beijing 100191, China; [10]Chinese Academy of Medical Sciences & Peking Union Medical College, Beijing 100730, China; [11]Center for Excellence in Brain Science and Intelligence Technology, Chinese Academy of Sciences, Shanghai 200031, China and [12]National Resource Center for Non-Human Primates (Kunming), Primate Research Center at IBP (Beijing), Chinese Academy of Sciences, Beijing 100101, China

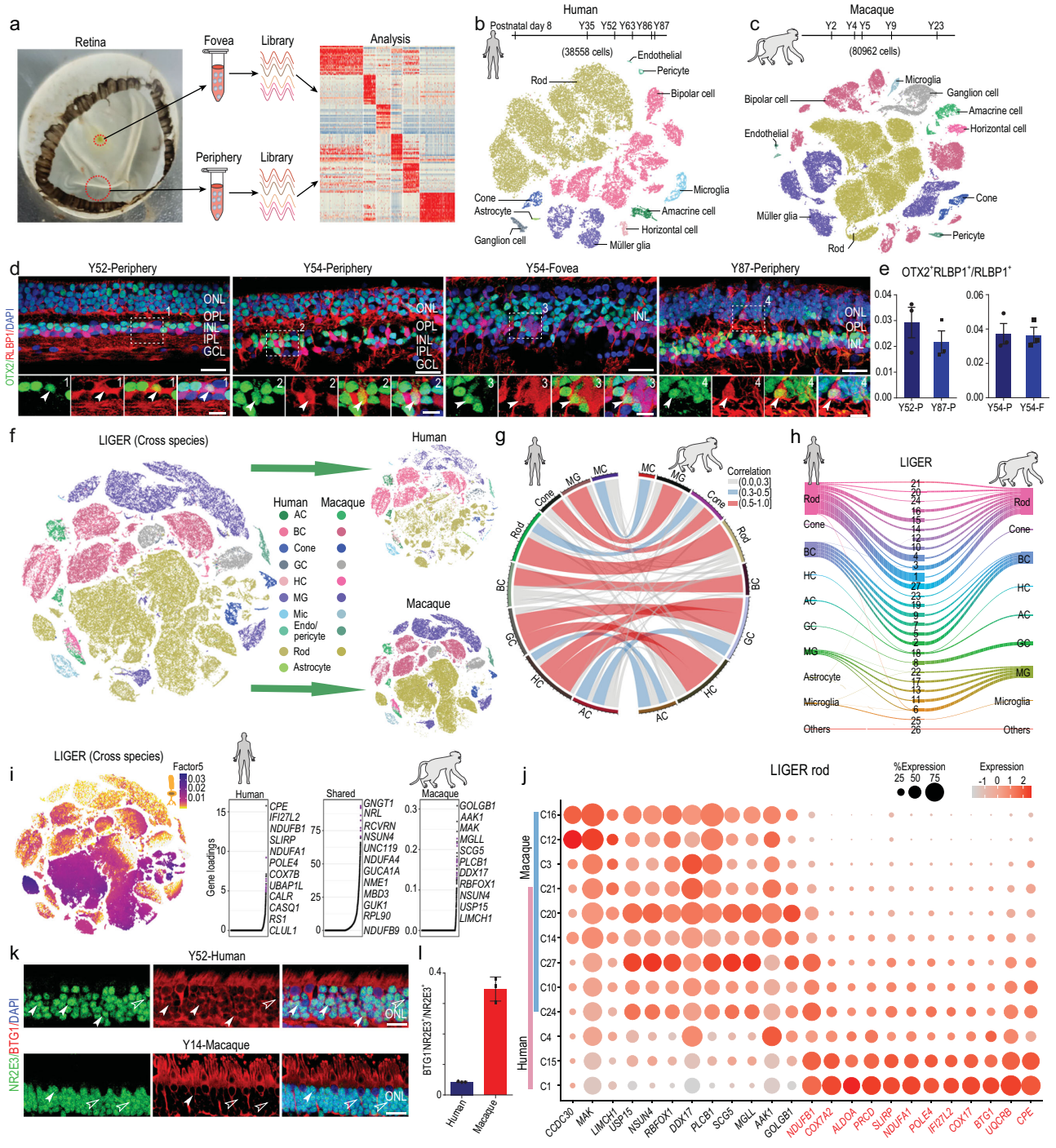

Figure 1. Cross-species transcriptome comparison of single-cell transcriptome profiles between human and macaque retina. (a) Experimental workflow for single-cell RNA-seq of human and macaque retina. Retinae were separated into foveal and peripheral samples for single-cell RNA-seq analysis. (b and c) t-SNE plot of single cells from human (b) and macaque (c) retina labelled with cell types. We obtained 38,558 human cells (samples: D8, Y35, Y52, Y63, Y86 and Y87) and 80,962 macaque cells (samples: Y2, Y4, Y5, Y9 and Y23). (d) Staining of OTX2 and RLBP1 of adult human retina in different age and region. Green: OTX2, red: RLBP1, blue: DAPI; bottom panel is higher-magnification view of top region boxed; solid arrowheads indicate double positive cell. Scale bars: 25 μm (top) and 10 μm (bottom). Experiments were repeated three times independently with similar results. (e) Bar charts showing proportion of OTX2$^+$RLBP1$^+$ cells out of RLBP1$^+$ cells in human adult Y52 peripheral, Y87 peripheral, Y54 peripheral and Y54 foveal retina, related to Fig. 1d. Data are means ± s.e.m.. Each sample was counted from three different slices. (f) t-SNE visualization of 119,520 single cells analyzed by LIGER, color-coded by cell type. Top right is human and bottom right is macaque, with each dot representing a single cell (AC: amacrine cell, BC: bipolar cell, GC: ganglion cell, HC: horizontal cell, MG: Müller glia, Mic: microglia, Endo: endothelial). (g) Circos plot showing cross-species mapping between retinal cell types from humans and macaques. Correlation coefficients are expressed by width and color. Gray indicates correlation coefficient below 0.3,

Figure 1. (*Continued.*) blue indicates correlation coefficient between 0.3 and 0.5, and red represents value greater than 0.5. (h) River plots comparing cell-type assignments for humans and macaques with LIGER joint clusters. (i) Cell factor loading values (left) and gene loading plots (right) of left loading dataset-specific and shared genes for factor 5. (j) Dot plot for specific genes related to factor 5 and differentially expressed genes (DEGs) of human and macaque rods in LIGER joint clusters, defined as rods. Macaque-specific genes are in black; human-specific genes are in red. Color of each dot shows average scale expression, and its size represents percentage of cells in cluster. (k) Immunostaining of NR2E3 and BTG1 in adult human and macaque retina. Solid arrowheads indicate $BTG1^{+}NR2E3^{+}$ cells, empty arrowheads indicate $BTG1^{-}$ $NR2E3^{+}$ cells. Scale bar: 15 μm. (l) Quantification of the proportion of $BTG1^{-}NR2E3^{+}$ cells in adult human and macaque retina related to Fig. 1k. Each sample was counted from three different slices. Data are means ± s.e.m..

respectively) showed similar transcriptomic profiles, with high expression of *OTX2* and *RLBP1* (Supplementary Fig. 1e). *OTX2* is a homeodomain transcription factor expressed in early and mature photoreceptors [5,11], and *RLBP1* is a marker for MGs [20]. These two markers have not been found co-expressed in retinal cells previously. To validate the existence of the subtypes, we performed immunofluorescence staining and observed that ∼3% of $RLBP1^{+}$ cells also expressed *OTX2* in the human adult retina, in both foveal and peripheral regions (Fig. 1d and e), indicating the existence of these cells in the adult human retina. Therefore, Clusters 46 and 51 are previously unidentified retinal cell types. In the macaque dataset, 68 clusters were classified, and 10 major cell types were annotated (Fig. 1c, Supplementary Fig. 1f and g, Supplementary Table 3). Compared to humans, astrocytes were not detected in the macaque retina (Fig. 1c, Supplementary Fig. 1f and g), consistent with previous scRNA-seq results from *M. fascicularis* [3]. Thus, we identified all major retinal cell types and $OTX2^{+}RLBP1^{+}$ cells in the primate retina by scRNA-seq analysis.

Cross-species transcriptome comparison between human and macaque retina

To investigate the similarities and differences between the human and macaque retina, we integrated and analyzed the single-cell transcriptomic profiles to perform cross-species comparison using the LIGER algorithm [21], which can identify shared- or specific-'factors,' a cluster of genes that define specific cell types (Fig. 1f, Supplementary Fig. 1h). The major cell types showed high correlations between the two species, suggesting conservativeness between humans and macaques. In addition, GCs and HCs exhibited similar transcriptomes (Fig. 1g), which is possibly a result of their close relationship in development [22]. The LIGER joint clustering assignments indicated that rod clusters showed species-related differences, although they were well-mixed in the tSNE plots (Fig. 1f and h). Clusters 1, 4 and 15 were human-dominant, whereas Clusters 3, 12 and 16 were macaque-dominant (Fig. 1h). We next plotted the species-specific dimorphic genes derived from particular rod clusters (factor 5) in LIGER analysis (Fig. 1i). General rod marker genes (*GNGT1* and *NRL*) were shared, but species-specific genes for rod clusters in humans (*CPE*, *IFI27L2* and *NDUFB1*) and macaques (*GOLGB1*, *AAK1* and *MAK*) were also identified (Fig. 1i). Further analysis indicated that these genes also showed cluster specificity, consistent with species preference (Fig. 1j). For example, *CPE* (carboxypeptidase E), which is required for the maturation of photoreceptor synapse and its signal transmission to the inner retina [23], was highly expressed in human-specific clusters (Clusters 1 and 15) but minorly expressed in some shared clusters (Clusters 10 and 24) (Fig. 1j). To validate the species-specific marker (Fig. 1j), we stained BTG1, a cell cycle inhibitory gene [24], in both human and macaque retina (Fig. 1k and l). The results showed that BTG1 co-localized with $NR2E3^{+}$ rods in outer nuclear layer (ONL) retina. However, the ratio of $BTG1^{-}NR2E3^{+}$ cells to $NR2E3^{+}$ cells was much lower in human retina, which is consistent with the scRNA-seq data. Although clusters of the cones and GCs from humans and macaques were closely matched by LIGER assignments (Clusters 23 and 8), we still found several species-specific genes in the cones (factor 18) and GCs (factor 6), respectively (Supplementary Fig. 1i). Collectively, our data demonstrated transcriptome conservativeness between the two species, but divergent gene expression was also discovered.

Distinct subtypes of primate rod photoreceptors

Rods are the dominant cell type in the mammalian retina and are responsible for vision under low-light intensity [1]. In total, we collected 16,686 rods in human retinal samples. As rods showed the highest interspecies differences by LIGER analysis, we next precisely analyzed rod subtypes. We first removed rod subclusters with more than 98% cells from the 8-day retinal sample to eliminate the influence of development. Based on analysis of differentially expressed genes (DEGs), human rods could be divided into two subgroups based on *MYO9A* expression (Fig. 2a and b). *CPE*, which was found

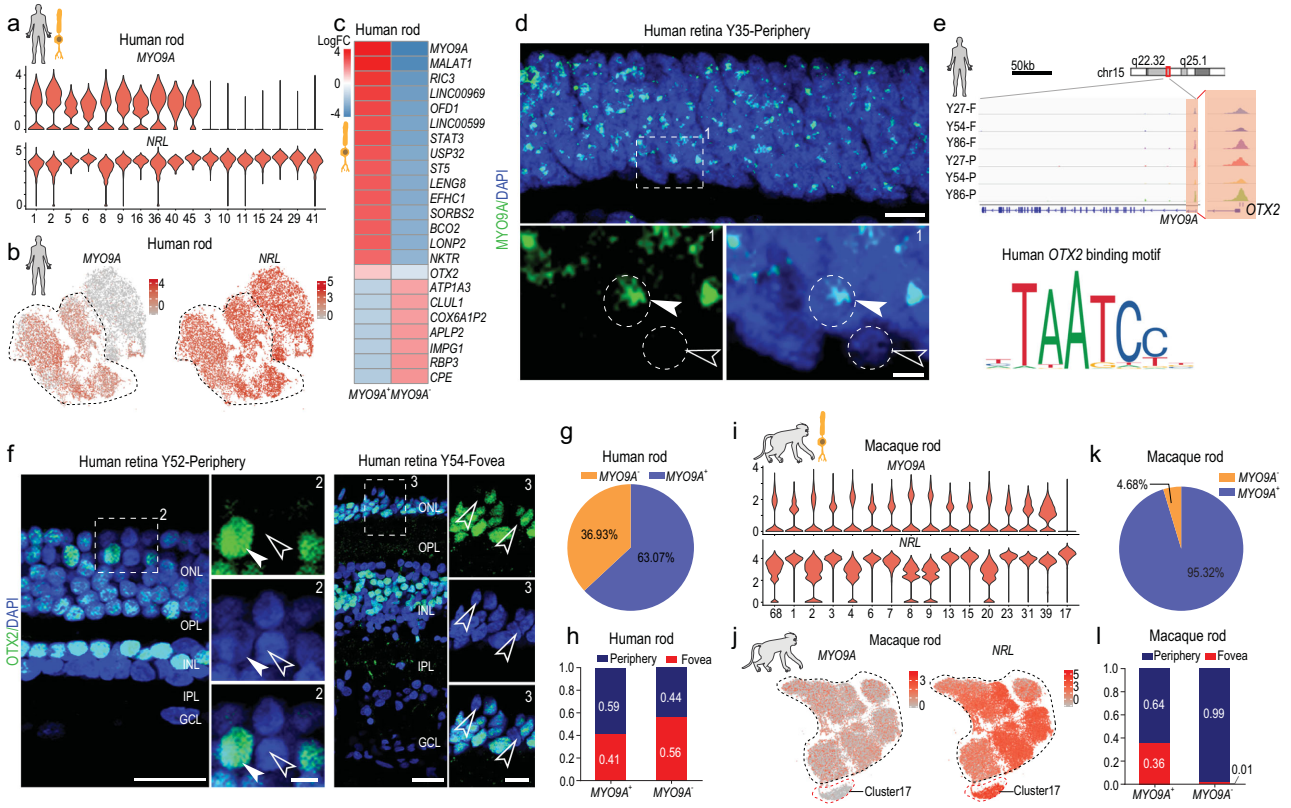

Figure 2. Distinct subtypes and differences in rods among primates. (a) Violin plots depicting expression of marker genes *MYO9A* and *NRL*, distinguishing 17 rod subclasses in human adult retina. (b) Visualization of expression of known marker genes *MYO9A* and *NRL* by t-SNE in human adult retina. Cells are colored according to gene expression levels (red, high; gray, low). (c) Heatmap illustrating log2 fold changes of differentially expressed genes (DEGs) between *MYO9A*$^+$ and *MYO9A*$^-$ rod subclasses in human adult retina. (d) *In situ* RNA hybridization of *MYO9A* in adult human retina. Arrowheads and dotted circles show positive and negative cells, respectively; solid arrowhead indicates positive cell, and empty arrowhead indicates negative cell. Blue, DAPI (nucleus marker). Scale bars: 10 μm (top) and 5 μm (bottom). Experiments were repeated three times independently with similar results. (e) Normalized ATAC-seq profiles of *MYO9A* in fovea and periphery of Y27, Y54 and Y86 retina samples showing activation of *MYO9A*. Amplifying panel shows predicted *OTX2* binding sites (top). DNA binding motif of *OTX2* (bottom), identified in ATAC-seq peaks close to *MYO9A* transcription start site (TTS). (f) Immunostaining of OTX2 in adult human peripheral (left) and foveal retina (right). Solid arrowheads indicate positive cells; empty arrowheads indicate negative cells. Scale bars: 25 μm (left) and 5 μm (right). Experiments were repeated three times independently with similar results. (g) Pie chart showing distribution of *MYO9A*$^+$ and *MYO9A*$^-$ subclasses in human adult retina samples. (h) Bar chart showing regional distributions of *MYO9A*$^+$ and *MYO9A*$^-$ rod subclasses in human retina samples. (i) Violin plots depicting expression of marker genes *MYO9A* and *NRL*, distinguishing 16 rod subclasses in macaque adult retina. (j) Visualization of expression of *MYO9A* and *NRL* by t-SNE in macaque retinae. Cells are colored according to gene expression levels (red, high; gray, low). (k) Pie chart showing distribution of *MYO9A*$^+$ and *MYO9A*$^-$ subclasses in macaque adult retina samples. (l) Bar chart showing regional distributions of *MYO9A*$^+$ and *MYO9A*$^-$ rod subclasses in macaque retina samples.

to be dominantly expressed in humans by cross-species comparison (Fig. 1i), was highly expressed in *MYO9A*$^-$ rods (Fig. 2c). In the human peripheral retina ONL, over 95% of cells were rods. Thus, we performed *MYO9A* RNAscope *in situ* hybridization (ISH) of the human peripheral retina and validated that a proportion of human rods expressed *MYO9A* (Fig. 2d), suggesting that human rods consist of *MYO9A*$^+$ and *MYO9A*$^-$ cells. Consistent with human retina, macaque rods also consist of *MYO9A*$^+$ and *MYO9A*$^-$ cells (Supplementary Fig. 2b). Moreover, a subcluster of *MYO9A*$^-$ in macaque retina was much lower than that in humans. To investigate the transcriptional regulation of *MYO9A*, bulk ATAC-seq was performed in human foveal and peripheral retinal samples (27, 54 and 86 years old). By searching transcription factor motifs from ATAC-seq peaks close to the *MYO9A* transcription start site (TSS), we found two potential OTX2 binding sites in *MYO9A* gene (Fig. 2e). Consistently, in humans, *OTX2* was generally expressed in the *MYO9A*$^+$ subcluster of rods (Fig. 2c, Supplementary Fig. 2a). Considering *OTX2* is a transcription factor controlling retinal photoreceptor cell fate [22], our results indicate that the expression of *MYO9A* might be regulated by *OTX2*. Accordingly, we observed both *OTX2*-positive and -negative cells in the human (Fig. 2f) and macaque retina (Supplementary

Fig. 2c), similar to the division of *MYO9A*. From the scRNA-seq data, we found a similar *MYO9A*$^{+}$ to *MYO9A*$^{-}$ rod ratio in the foveal and peripheral regions (Fig. 2g and h). As rods showed species specificity in their transcriptomes, we analyzed the macaque rods (36,904 cells) and observed that one subcluster (4.7% rods) was *MYO9A*$^{-}$, which was much lower than that in humans (36.9%) (Fig. 2i–k) and consistent with ISH data (Supplementary Fig. 2b). Additionally, the distribution of *MYO9A*$^{-}$ rods showed regional preference, with 98.6% of *MYO9A*$^{-}$ rods located in the peripheral retina in macaques (Fig. 2l). Taken together, though the rods of humans and macaques could both be divided into two subtypes based on *MYO9A* expression, the proportion and location of *MYO9A*$^{-}$ cells differed substantially between the two species.

BCs are neurons that connect the outer to the inner layer in the retina, and play direct or indirect roles in transmitting signals from photoreceptors to GCs [1]. We found 17 and 18 BCs subclusters in humans and macaques, respectively, and categorized these subclusters into 12 and 11 known types in humans and macaques, respectively (Supplementary Fig. 2d–f). The 11 types of *M. mulatta* BCs were consistent with previous findings in *M. fascicularis* [3]. Similar to *M. fascicularis*, the Blue Bipolar (BB) and Giant Bipolar (GB) types were grouped together because of their transcriptional similarity in *M. mulatta*, whereas BB and GB types of human BCs could be separated by the transcriptome with distinct molecular markers (Supplementary Fig. 2e). However, the BC subtypes were generally conserved between humans and macaques (Supplementary Fig. 2g).

Regionally different transcriptomes of primate MGs and cones

The foveal retina is cone-dominated, whereas the peripheral retina is rod-dominated. MGs are particularly important in the fovea because the foveola center is formed only by cone and MG processes. To investigate the region-specific features of MGs and cones, we compared their single-cell transcriptomes in the foveal and peripheral retina. MGs exhibited remarkable regional specificity (Fig. 3a). Generally, most foveal MGs were cells in Clusters 13 and 22 (Fig. 3a) and exhibited high *TRH*, *FGF9*, *DIO2*, *CYP26A1*, *RGR* and *HTRA1* expression (Fig. 3b, Supplementary Fig. 3a and b). The majority of MGs in Clusters 21, 32 and 43 were located in peripheral retina and exhibited high *NPVF*, *MT3*, *MT2A* and *GPX3* expression (Fig. 3b, Supplementary Fig. 3a and b). Immunostaining of NPVF and RLBP1 in the human retina validated the scRNA-seq results, indicating that *NPVF* was a marker gene of peripheral MGs in humans (Fig. 3c). In addition, immunostaining and ISH also revealed the foveal MG specific expression of TRH (thyrotropin releasing hormone) and DIO2 (iodothyronine deiodinase 2), respectively (Fig. 3d and e). We performed weighted gene co-correlation network analysis (WGCNA) of MG regional DEGs and found several foveal and peripheral MG-specific modules (Supplementary Fig. 3c and d). For the top foveal module, we performed network analysis and found that *TRH*, *RGR*, *DIO2* and *CYP26A1* were also highly enriched (Fig. 3f). CYP26A1 is a retinoic acid-metabolizing enzyme, with foveal-specific expression validated here (Supplementary Fig. 3e). *CYP26A1* has been identified as a DEG of the foveal retina during human development [25], which functions in rod-free zone generation [26,27]. Interestingly, the expression level of *RGR* (retinal G protein-coupled receptor), another foveal MG-specific gene, is higher in the foveal MGs. *RGR* encodes a crucial factor for the photic visual cycle of cone visual pigment regeneration, mutations of which are associated with retinitis pigmentosa (RP) [28]. The cone visual cycle of regenerating 11-*cis* retinal is dependent on both retinal pigment epithelium (RPE) and MGs [28,29]. Thus, the higher *RGR* expression in the foveal MGs might meet the high demand of cone visual pigment regeneration in the cone-dominated fovea. Additionally, *HTRA1* (high-temperature requirement protein A1), a risk factor gene of AMD, exhibited high expression in the fovea MGs, consistent with the fovea being more vulnerable in AMD [30]. Together, our results indicated that MGs in the fovea, as a type of supporting glial cell, expressed specific genes for facilitating cone photoreceptor regeneration, specification and functional maintenance. We next analyzed the MGs of macaques, which also showed regional differences in terms of cell types and gene expression patterns (Supplementary Fig. 3f and g). Comparing the DEGs between the foveal and peripheral MG across both species, several genes showed similar regional specificity, for example *TRH*, *DIO2*, *CYP26A1*, *RGR*, *GPX3* and *RPL7*, whereas gene expression preference of *NPVF*, *MT1F* and *JUNB* was not conserved (Fig. 3g).

Interestingly, cone photoreceptors also exhibited remarkable region-specificity in both humans and macaques (Fig. 3h). The thyroid hormone (TH) receptor, THRβ (human thyroid hormone receptor beta), is expressed in cones and also serves as a transcription factor [31]. Our ATAC-seq results showed that the potential binding sites of THRβ were found in open chromatin close to the TSS of several foveal-enriched genes (*RFC1*, *POLE4* and

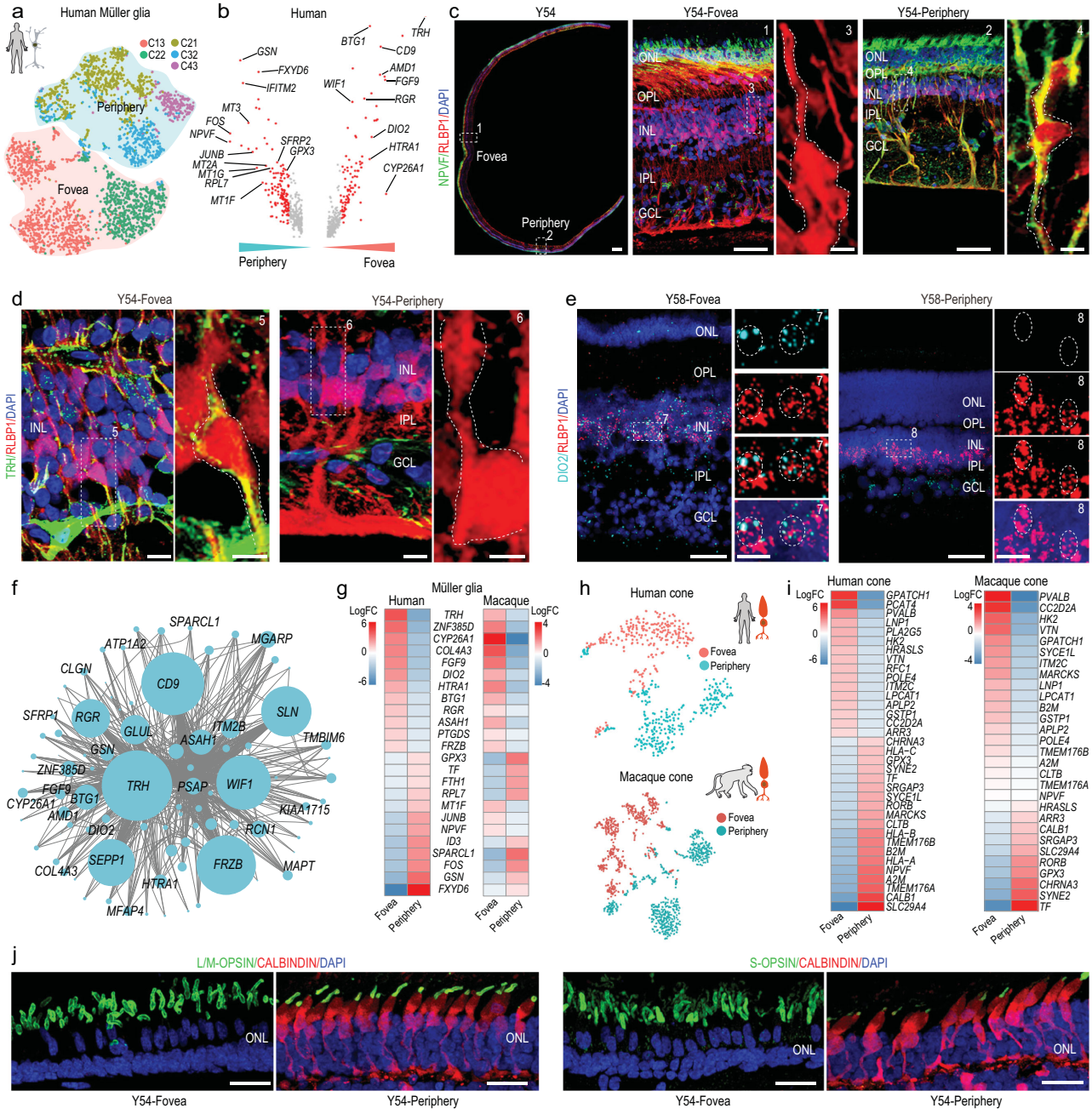

Figure 3. Regionally different transcriptomes of primate MG and cones. (a) t-SNE plot of MG distinguished by different subclasses (dots, individual cells; color, subclasses; color contours, regions). (b) Volcano plot of DEGs between human foveal and peripheral MG. Red dots show average log2 fold changes >0.5. (c) Immunostaining of RLBP1 and NPVF in Y54. Middle panel is higher magnification view of fovea in left-most panel; right panel is higher-magnification view of periphery in left-most panel. Scale bar of Y54: 300 μm, 50 μm (middle), 5 μm (middle on right), 50 μm (right), 5 μm (right-most). Experiments were repeated three times independently with similar results. (d) Immunostaining of RLBP1 and TRH in Y54 human retina, Scale bars: 10 μm (left) and 5 μm (right). Experiments were repeated three times independently with similar results. (e) *In situ* RNA hybridization of *DIO2* and *RLBP1* in Y58 human retina. Blue, DAPI (nucleus marker). Scale bars: 50 μm (left) and 10 μm (right). Experiments were repeated three times independently with similar results. (f) Network analysis of blue module genes. (g) Heatmap illustrating log2 fold changes of DEGs related to human foveal and peripheral Müller glia in human and macaque adult retina. (h) t-SNE plot of human (top) and macaque (bottom) cones based on regions (dots, single cell; color, regions). (i) Heatmap showing log2 fold changes in DEGs between foveal and peripheral cones in human (left) and macaque (right) adult retina. (j) Immunostaining of S-OPSIN/CALBINDIN and L/M-OPSIN/CALBINDIN in Y54. Scale bar: 25 μm. Experiments were repeated three times independently with similar results.

APLP2) (Fig. 3i, Supplementary Fig. 3h). DIO2 converts the inactive TH thyroxine (T4) in blood into the active TH triiodothyronine (T3) [32]. Of note, we also found *DIO2* to be highly expressed in foveal MGs (Fig. 3b and e), indicating that foveal MGs may regulate the region-specific transcriptome of cones. The dosage of TH has been reported to play a role in specifying cone subtypes in human retinal organoids [33]. Here, our data demonstrated that MGs might modulate region-specific gene expression by TH signaling in foveal cones in adulthood. *CALB1* was one of the markers for peripheral cones, as determined by scRNA-seq data analysis (Fig. 3i). To confirm this finding, we carried out immunostaining of cone OPSIN and CALBINDIN (encoded by gene *CALB1*) in human retina and found that CALBINDIN was only expressed in cones (both L/M and S cones) located in the peripheral retina (Fig. 3j, Supplementary Fig. 3i). Taken together, both MGs and cones displayed distinct regional gene expression profiles and MGs may modulate region-specific gene expression to facilitate cone photoreceptor generation, specification and functional maintenance by cell-cell communication.

Molecular classification of retinal HCs in primates

HCs are located in the inner nuclear layer (INL) of the vertebrate retina, where they interconnect laterally with photoreceptors. Here, the human HCs clustered into classical H1 (*LHX1*$^+$ *PCP4*$^+$) and H2 (*ISL1*$^+$ *CALB1*$^+$) subtypes (Fig. 4a and b, Supplementary Fig. 4a). Interestingly, H1 and H2 cell types showed regional preference, i.e. 92.0% of foveal HCs were H1 type and 60% of peripheral HCs were H2 type (Fig. 4c). Immunostaining of CALBINDIN/ONECUT2, and ISH of *LHX1* and *ISL1* in the human retina confirmed the scRNA-seq results, illustrating that most of the human foveal HCs were H1 (Fig. 4d–f). The macaque HCs were also classified as H1 and H2 types (Fig. 4g, Supplementary Fig. 4b). Compared to the 92.0% in humans, 60.0% of macaque foveal HCs were H1 type (Fig. 4h). Although most DEGs between H1 and H2 showed similar expression across the two primate species, some human H1-enriched genes, e.g. *FILIPL1*, *CMSS1* and *PCDH9*, were highly expressed in macaque H2 cells, whereas some human H2-enriched genes, e.g. *SYNPR*, *MGARP* and *AKR1B1*, were highly expressed in macaque H1 cells (Fig. 4i, Supplementary Fig. 4c), indicating that distribution and gene expression were slightly different across the H1/H2 cell types of both species.

Aging patterns of human retina

Aging affects retinal function and structure physiologically and pathologically. To clarify the cellular and molecular changes during aging, we systematically studied human retinal samples (between 35 and 87 years old). We categorized the five samples into three groups (35Y, adult group; 52Y and 63Y, mid-age group; 86Y and 87Y, aging group). We first focused on whether the genes continuously increased or decreased from the adult to aging groups (Fig. 5a–e). In total, the expression of 87 genes was up-regulated. Gene ontology (GO) analysis indicated these genes may play roles in response to hypoxia, regulation of cell death, microglial cell activation (Fig. 5a and b, and Supplementary Table 4). Interestingly, some up-regulated genes only increased in certain cell types. For example, *LIN7A* and *CALD1* were only elevated in cones with aging (Fig. 5c). Additionally, 121 genes related to visual perception, phototransduction, adenosine triphosphate (ATP) biosynthetic process and retinoid metabolic processes, were down-regulated with aging (Fig. 5d and e, Supplementary Table 4), indicating that visual function is affected as retina ages. We also analyzed the age-related GO change in each cell subtype (Supplementary Fig. 5a–h). Interestingly, in the GO analysis for each cell type, we found that most retinal neurons showed similar GOs to total retinal cells (Fig. 5b), such as response to hypoxia, response to oxidative stress and regulation of cell death. In contrast, GOs in MG are anti-apoptosis, negative regulation of programmed cell death and response to hypoxia. These data suggest that retinal cells are heterogeneous during aging. The GO analysis suggested that MG might be in anti-apoptosis status to prevent retinal neuron death during aging. Consistently, among the neurons, a dramatic decrease in rod photoreceptors with retinal aging was observed by scRNA-seq data and immunostaining analysis (Fig. 5f and g), but there was no dramatic cell number change of BCs (Supplementary Fig. 5i and j). Rod outer segments, which are specialized compartments of photoreceptor for phototransduction, were greatly decreased with RHO protein (Fig. 5g). In addition, RHO protein was ectopically expressed in cell bodies, indicating defective light-sensing function of aged rod photoreceptors. In retinal glial cells, the proportion of microglia was remarkably increased in the aged samples (Fig. 5f and h), consistent with the up-regulated genes, which were enriched in response to hypoxia and microglial cell activation (Fig. 5b). Interestingly, the major changes in age-related cell-type proportion in humans were not obvious in the macaque retina (Fig. 5f).

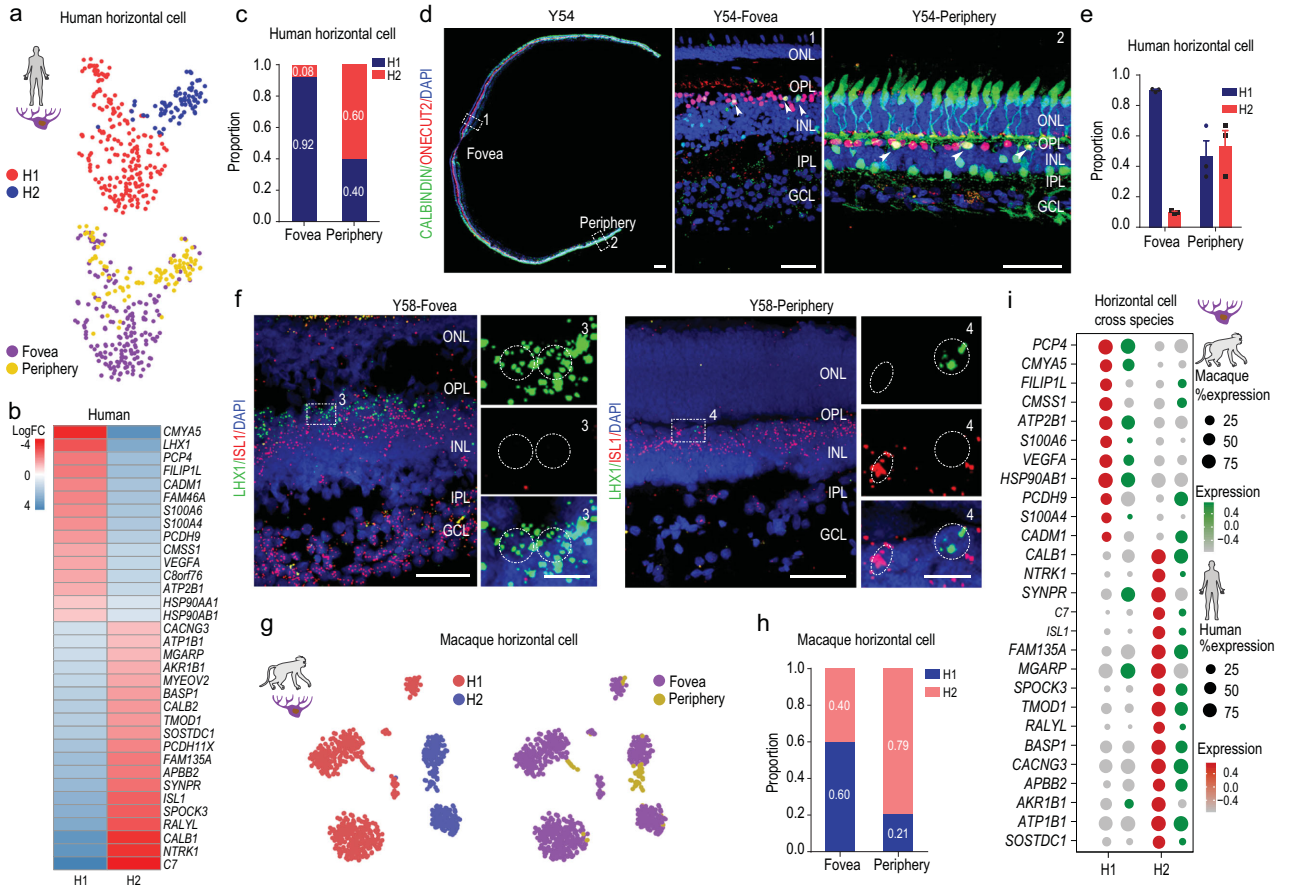

Figure 4. Molecular properties of retinal horizontal cells in primates. (a) t-SNE plot of human horizontal cells, colored by subclass (top) and region (bottom). Each dot is a single cell. (b) Heatmap showing log2 fold changes in DEGs between H1 and H2 horizontal cells in human adult retina. (c) Proportion of human horizontal cell subclasses in foveal and peripheral regions. (d) Immunostaining of CALBINDIN and ONECUT2 in Y54. Middle panel is higher-magnification view of fovea in left-most panel; right panel is higher-magnification view of periphery in left-most panel. Solid arrowheads indicate double positive cell. Scale bars of Y54: 300 μm, 50 μm (middle) and 50 μm (right). Experiments were repeated three times independently with similar results. (e) Quantification of proportion of H1 and H2 subclasses in foveal and peripheral human adult retina related to Fig. 4d. Each sample was counted from three different slices. Data are means ± s.e.m.. (f) *In situ* RNA hybridization of *LHX1* and *ISL1* in Y58 human retina. Blue, DAPI (nucleus marker). Scale bars: 50 μm (left) and 10 μm (right). Experiments were repeated three times independently with similar results. (g) t-SNE visualization of macaque horizontal cells, color-coded by subclass (left) and region (right). Each dot represents a single cell. (h) Proportion of macaque horizontal cell subclasses in foveal and peripheral regions. (i) Dot plot showing H1- and H2-specific marker genes in human (red) and macaque (green) adult retina. Size of each dot represents percentage of cells in each cluster (red/green, high expression; gray, low expression).

As two major classes of rods were identified in humans (*MYO9A*$^+$ and *MYO9A*$^-$) (Fig. 2) and rods were the most vulnerable cell type during aging, we next asked whether these two types of rods were differentially affected by aging. Quantification analysis of scRNA-seq data indicated that the population of *MYO9A*$^-$ rods dramatically decreased during aging (Fig. 5i), which was confirmed by the ISH of *MYO9A* in the human peripheral retina ONL (Fig. 5j). To further validate the reduction of *MYO9A*$^-$ rods, we quantified the ratio of *MYO9A*$^+$ and *MYO9A*$^-$ cells to the total retinal cells in different ages of human retinae (Supplementary Fig. 5k). The data revealed that both *MYO9A*$^+$ and *MYO9A*$^-$ cells were reduced along aging. Moreover, the proportion of *MYO9A*$^-$ cells was much more dramatically reduced in aged human retina than was *MYO9A*$^+$ cells. Thus, it appeared that human *MYO9A*$^+$ rods were more resistant to aging. Because the macaque rods were predominately *MYO9A*$^+$ (95.4%), we did not observe obvious changes in the proportions of *MYO9A*$^+$ and *MYO9A*$^-$ rods in macaque retina during aging (Fig. 5i). As *OTX2* potentially regulates *MYO9A* expression in human rods (Fig. 2e), we next explored *OTX2* expression in the human peripheral retina ONL. Unsurprisingly, *OTX2*$^+$ cells in the peripheral ONL increased from 62.1% at 54 years old to 96.7% at 87 years old (Fig. 5k and l). Together, we identified a cell-type-specific degeneration of

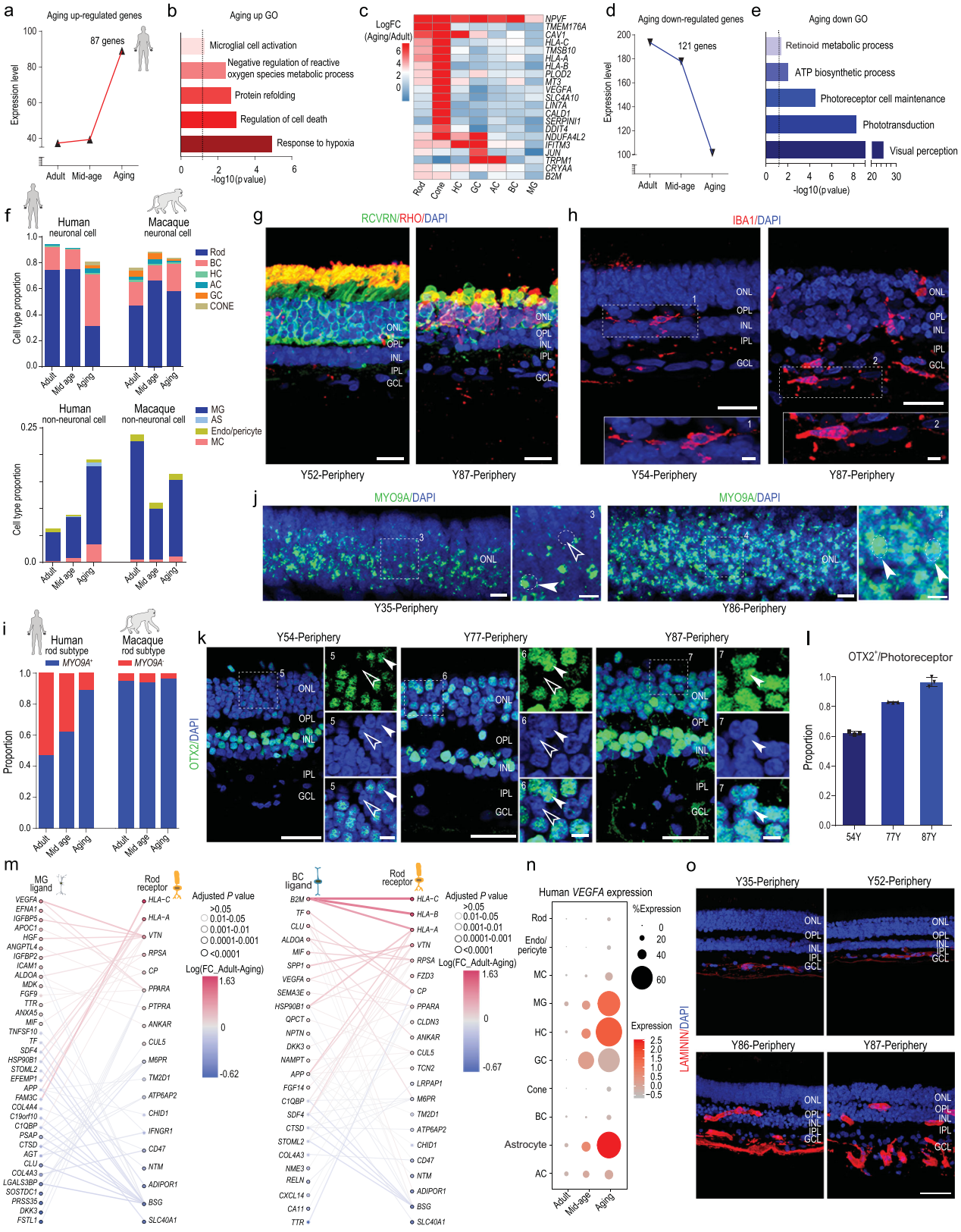
a
Aging up-regulated genes
87 genes
Expression level
Adult
Mid-age
Aging
b
Aging up GO
Microglial cell activation
Negative regulation of reactive oxygen species metabolic process
Protein refolding
Regulation of cell death
Response to hypoxia
-log10(p value)
c
LogFC (Aging/Adult)
NPVF
TMEM176A
CAV1
HLA-C
TMSB10
HLA-A
HLA-B
PLOD2
MT3
VEGFA
SLC4A10
LIN7A
CALD1
SERPINI1
DDIT4
NDUFA4L2
IFITM3
JUN
TRPM1
CRYAA
B2M
Rod
Cone
HC
GC
AC
BC
MG
d
Aging down-regulated genes
121 genes
Expression level
Adult
Mid-age
Aging
e
Aging down GO
Retinoid metabolic process
ATP biosynthetic process
Photoreceptor cell maintenance
Phototransduction
Visual perception
-log10(p value)
f
Human neuronal cell
Macaque neuronal cell
Cell type proportion
Rod
BC
HC
AC
GC
CONE
Human non-neuronal cell
Macaque non-neuronal cell
MG
AS
Endo/pericyte
MC
Adult
Mid age
Aging
g
RCVRN/RHO/DAPI
ONL
OPL
INL
IPL
GCL
Y52-Periphery
Y87-Periphery
h
IBA1/DAPI
Y54-Periphery
Y87-Periphery
j
MYO9A/DAPI
Y35-Periphery
Y86-Periphery
i
Human rod subtype
Macaque rod subtype
MYO9A+
MYO9A-
Proportion
k
Y54-Periphery
Y77-Periphery
Y87-Periphery
OTX2/DAPI
l
OTX2+/Photoreceptor
Proportion
54Y
77Y
87Y
m
MG ligand
Rod receptor
Adjusted P value
>0.05
0.01-0.05
0.001-0.01
0.0001-0.001
<0.0001
Log(FC_Adult-Aging)
BC ligand
n
Human VEGFA expression
%Expression
Expression
Rod
Endo/pericyte
MC
MG
HC
GC
Cone
BC
Astrocyte
AC
o
Y35-Periphery
Y52-Periphery
Y86-Periphery
Y87-Periphery
LAMININ/DAPI

Figure 5. Molecular characteristics of aging primate retina and aging-related changes in cell-cell communication. (a) Co-expression patterns of up-regulated genes among aging stages. (b) Enriched gene ontology terms of up-regulated genes. (c) Heatmap illustrating log2 fold changes of up-regulated genes to cell types at different aging stages in human adult retina. (d) Co-expression patterns of down-regulated genes among aging stages. (e) Enriched gene ontology terms of down-regulated genes. (f) Neuronal or non-neuronal cell proportions of human and macaque adult retina at different aging stages. (g and h) Immunostaining of RCVRN/RHO (g) in human retina of Y52 and Y87, IBA1 (h) of Y54 and Y87. Scale bars: 20 μm (g), 25 μm (h, top) and 5 μm (h, bottom). Experiments were repeated three times independently with similar results. (i) Proportion of rod subclasses (*MYO9A*$^{+}$ and *MYO9A*$^{-}$) in human adult retina at each stage. (j) *In situ* RNA hybridization of *MYO9A* in Y35 and Y86 human retina. Blue, DAPI (nucleus marker). Scale bars: 10 μm (left) and 5 μm (right). Experiments were repeated three times independently with similar results. (k) Immunostaining of OTX2 in human Y54, Y77 and Y87 peripheral retina. Solid arrowheads indicate positive cells; empty arrowheads indicate negative cells. Scale bars: 25 μm (left) and 5 μm (right). Experiments were repeated three times independently with similar results. (l) Quantification of *OTX2*$^{+}$ cells in outer nuclear layer (ONL) at various ages, related to Fig. 5k. Data are means ± s.e.m.. Each sample was counted from three different slices. (m) Aging-related ligands produced and secreted by MGs with receptors expressed in rods (left) and aging-related ligands produced and secreted by BCs with receptors expressed in rods (right). In all panels, nodes represent ligands or receptors expressed in denoted cell type, and edges represent protein-protein interactions between them. Node color represents magnitude of DEG. Edge color represents sum of scaled differential expression magnitudes from each contributing node, whereas width and transparency are determined by magnitude of scaled differential expression. These figures have been filtered such that top 100 edges representing most differentially expressed node pairs are shown. (n) Dot plot for *VEGF-A* expression in different cell types at each stage in human adult retina. Size of each dot represents percentage of cells in each cluster. Gray to red indicates gradient from low to high gene expression. (o) Confocal imaging of LAMININ in human Y35, Y52, Y86 and Y87 peripheral retina. Scale bars: 50 μm. Experiments were repeated three times independently with similar results.

rod subtypes and depicted gene-expression signatures for each retinal cell type during the process of aging.

Aging-related changes in cell-cell communication

Aging is a systematic continuous process, regulated by both intrinsic and external signals. To understand how intercellular communication plays a role in the aging of rods, we built a network of ligand-receptor interactions among different cell types and focused on the changes in ligand-receptor expression with aging (Fig. 5m, Supplementary Fig. 5l and m). We studied the ligand-receptor changes between rods and MGs or BCs (Fig. 5m, Supplementary Fig. 5m), as MGs and BCs closely interact with rods. Expression of VEGF-A, which are linked to AMD and retinal angiogenesis, were up-regulated in BCs and MGs. Their receptors also increased in rods with aging (Fig. 5m). Interestingly, VEGF-A expression was dramatically increased in MGs, HCs and astrocytes. Accordingly, abnormal angiogenesis was also observed in the aged retina (Fig. 5n and o, Supplementary Fig. 5n). The length of blood vessels was significantly increased in aged retina. Together, these findings indicate that aging could be a synergistic process with comprehensive changes in different types of neuronal or glial cells in the human retina.

Molecular changes in foveal and peripheral aged human retina

To investigate the aging trajectories of foveal and peripheral primate retina, we established aging scores using an aging-related gene set which was downloaded from Human Ageing Genomic Resources (https://genomics.senescence.info/). The methods used for aging score calculation were adapted from the algorithm used by Nowakowski to predict the maturation of cortical neurons [34] (see Methods). We found that the elevation trends of the aging score generally matched the real sample age (Fig. 6a). Of note, the foveal cells showed higher aging scores than peripheral cells, indicating that the fovea may be more vulnerable to aging. In addition, the increase in aging scores started after 52 years old (Fig. 6a), suggesting that the retinal aging process may gradually accelerate at middle age. To verify the reliability of the aging score, we first examined the expression trends of classical aging genes, and found that the expression levels of *STAT3* and *PIK3R1* were positively correlated with aging. However, the expression levels of *PCNA* and *GSTP1* were negatively correlated with aging, indicating that the aging score models by single-cell transcriptomic profiles were reliable (Fig. 6b, Supplementary Fig. 6a). We then focused on the expression of human aging up-regulated genes in the retina and found that *NPVF*, *GPX3*, *B2M*, *PCP4* and *CRYAA* were positively correlated with aging, whereas down-regulated genes *RHO*, *DRD4*, *GNGT1* and *MFG8* were negatively correlated with aging (Fig. 6c, Supplementary Fig. 6b and c, Supplementary Table 4).

As foveal and peripheral retina exhibited different degrees of aging (Fig. 6a), and MGs, cones, and HCs showed regional differences (see Figs 3 and 4), we investigated whether these regional differences changed during aging. *NPVF*, a highly expressed gene in peripheral MGs, was significantly up-regulated during aging based on the scRNA-seq

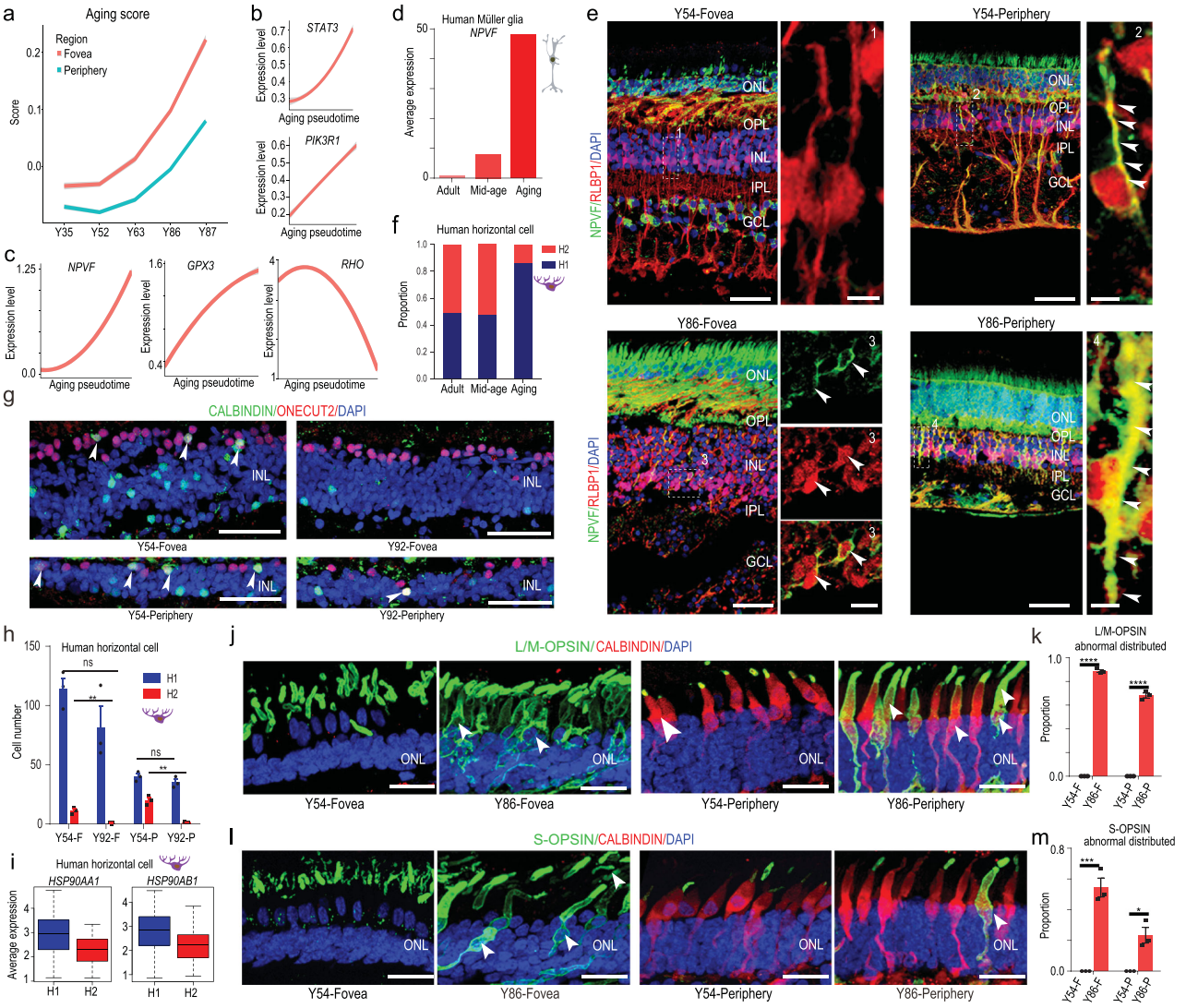

Figure 6. Region- and cell-type-specific molecular changes in aged human retina. (a) Pseudo-aging trajectories between fovea and periphery in human retina. The shadow represents the confidence interval (95%) around the fitted curve. (b) Trajectories of expression of classical human aging genes across human adult retina aging pseudotime. The shadow represents the confidence interval (95%) around the fitted curve. (c) Trajectories of expression of up- and down-regulated genes across human adult retina aging pseudotime. The shadow represents the confidence interval (95%) around the fitted curve. (d) Average expression of *NPVF* at different aging stages in Müller glia. (e) Immunostaining of RLBP1 and NPVF in Y54 and Y86. Solid arrowheads indicate double positive cell. Scale bars of Y54: 50 μm (left), 5 μm (right). Scale bars of Y86: 50 μm (left), 10 μm (right, fovea), 5 μm (right periphery). Experiments were repeated three times independently with similar results. (f) Cell proportions of human H1 and H2 subclasses at different aging stages. (g) Confocal images of adult human retina in Y52 and Y92. Green: CALBINDIN, red: ONECUT2, blue: DAPI. Solid arrowheads indicate double positive cell. Scale bar: 50 μm. Experiments were repeated three times independently with similar results. (h) Bar chart showing quantification of CALBINDIN/ONECUT2 immunostaining data, related to Fig. 6g. Data are means ± s.e.m.. *P* values calculated by two-sided *t*-test. n.s., no significance, $^{**}P < 0.01$. Each sample was counted from three different slices. (i) Boxplot for *HSP90AA1* and *HSP90AB1* in H1 and H2 subclasses. (j) Immunostaining of L/M-OPSIN/CALBINDIN in Y54 and Y86. Solid arrowheads indicate OPSIN translocation in soma. Scale bar: 25 μm. Experiments were repeated three times independently with similar results. (k) Bar chart showing quantification of Fig. 6j (data are means ± s.e.m., Y54-F VS Y86-F, $^{****}P < 0.0001$; Y54-P VS Y86-P, $^{****}P < 0.0001$). Each sample was counted from three different slices. (l) Immunostaining of S-OPSIN/CABINDIN in Y54 and Y86. Solid arrowheads indicate OPSIN translocation in soma. Scale bar: 25 μm. Experiments were repeated three times independently with similar results. (m) Bar chart showing quantification of Fig. 6l. Data are means ± s.e.m.. *P* values calculated by two-sided *t*-test. $^{*}P < 0.05$, $^{***}P < 0.001$. Each sample was counted from three different slices.

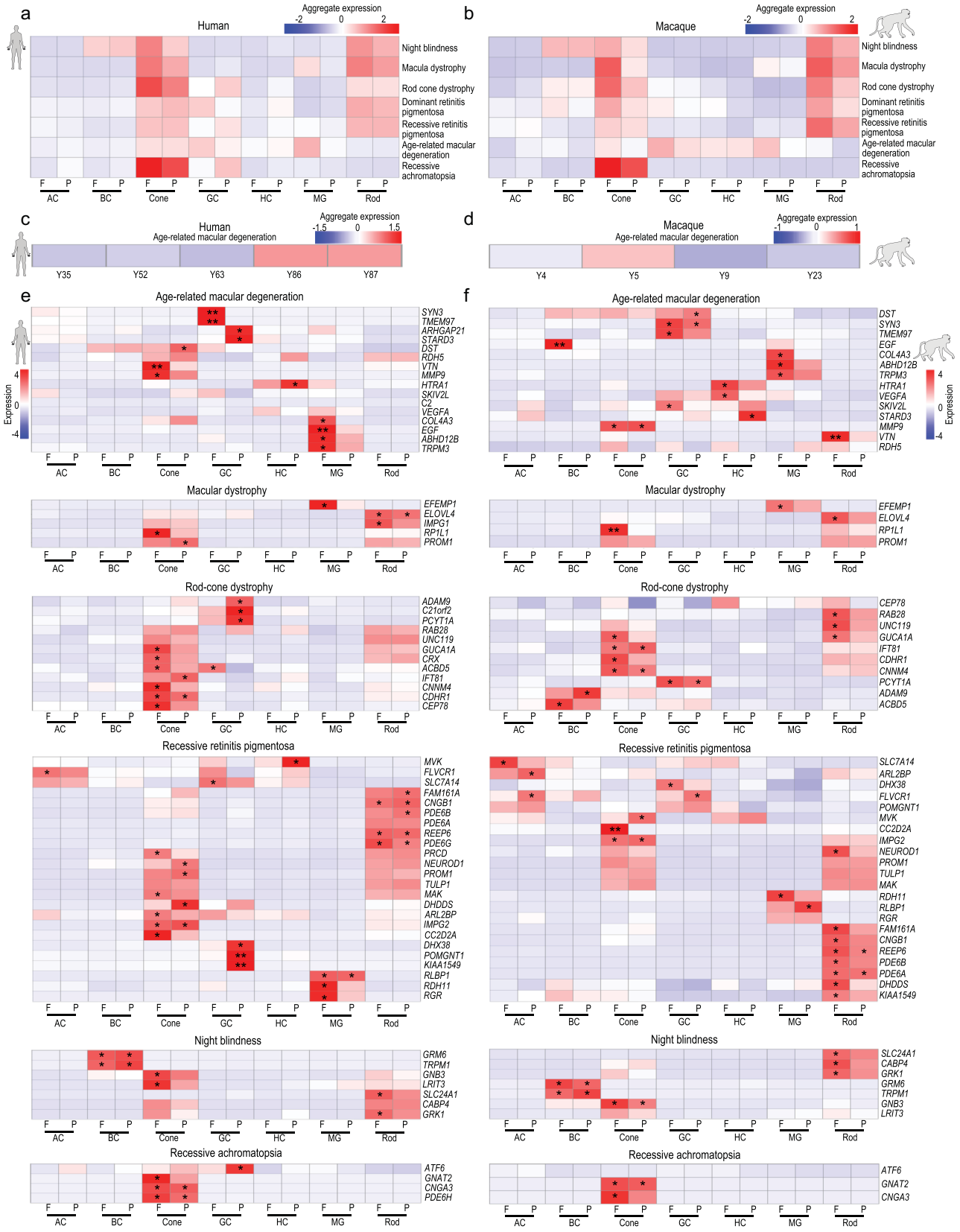
a
Human
Aggregate expression
-2
0
2
Night blindness
Macula dystrophy
Rod cone dystrophy
Dominant retinitis pigmentosa
Recessive retinitis pigmentosa
Age-related macular degeneration
Recessive achromatopsia
F P
AC
BC
Cone
GC
HC
MG
Rod
b
Macaque
c
Human
Age-related macular degeneration
-1.5
1.5
Y35
Y52
Y63
Y86
Y87
d
Macaque
-1
1
Y4
Y5
Y9
Y23
e
Age-related macular degeneration
SYN3
TMEM97
ARHGAP21
STARD3
DST
RDH5
VTN
MMP9
HTRA1
SKIV2L
C2
VEGFA
COL4A3
EGF
ABHD12B
TRPM3
Expression
4
0
-4
Macular dystrophy
EFEMP1
ELOVL4
IMPG1
RP1L1
PROM1
Rod-cone dystrophy
ADAM9
C21orf2
PCYT1A
RAB28
UNC119
GUCA1A
CRX
ACBD5
IFT81
CNNM4
CDHR1
CEP78
Recessive retinitis pigmentosa
MVK
FLVCR1
SLC7A14
FAM161A
CNGB1
PDE6B
PDE6A
REEP6
PDE6G
PRCD
NEUROD1
PROM1
TULP1
MAK
DHDDS
ARL2BP
IMPG2
CC2D2A
DHX38
POMGNT1
KIAA1549
RLBP1
RDH11
RGR
Night blindness
GRM6
TRPM1
GNB3
LRIT3
SLC24A1
CABP4
GRK1
Recessive achromatopsia
ATF6
GNAT2
CNGA3
PDE6H
f
Age-related macular degeneration
DST
SYN3
TMEM97
EGF
COL4A3
ABHD12B
TRPM3
HTRA1
VEGFA
SKIV2L
STARD3
MMP9
VTN
RDH5
Expression
4
0
-4
Macular dystrophy
EFEMP1
ELOVL4
RP1L1
PROM1
Rod-cone dystrophy
CEP78
RAB28
UNC119
GUCA1A
IFT81
CDHR1
CNNM4
PCYT1A
ADAM9
ACBD5
Recessive retinitis pigmentosa
SLC7A14
ARL2BP
DHX38
FLVCR1
POMGNT1
MVK
CC2D2A
IMPG2
NEUROD1
PROM1
TULP1
MAK
RDH11
RLBP1
RGR
FAM161A
CNGB1
REEP6
PDE6B
PDE6A
DHDDS
KIAA1549
Night blindness
SLC24A1
CABP4
GRK1
GRM6
TRPM1
GNB3
LRIT3
Recessive achromatopsia
ATF6
GNAT2
CNGA3

Figure 7. Region-, cell type-, and species-specific expression patterns of genes associated with human retinal diseases. (a and b) Aggregated expression of human eye disease-associated genes in human (a) and macaque (b) cell types, with some diseases showing obvious regional enrichment characteristics. (c and d) Aggregated expression of age-related macular degeneration-associated genes at different human (c) and macaque (d) ages. (e and f) Expression patterns of human eye disease-associated genes in human (e) and macaque (f) retinal cell types. *P* values were calculated by bootstrap hypothesis test, $^{*}P < 0.05$, $^{**}P < 0.01$.

dataset (Fig. 6d). Consistently, immunostaining of *NPVF* suggested its increased expression in peripheral MGs with aging. Interestingly, *NPVF* was ectopically expressed in the foveal MGs of 86-year-old retina, but not of 54-year-old retina (Fig. 6e). Additionally, we found that average expression of foveal MG-enriched genes gradually decreased during aging, indicating that the regional specificity of foveal MGs declined (Supplementary Fig. 6d). In contrast, the expression of peripheral MG-enriched genes did not show an obvious change trend during aging (Supplementary Fig. 6e).

Other than MGs, the proportion of H2-type HCs in humans decreased from 52.3% (mid-age) to 14.2% (aged) (Fig. 6f). However, this trend was not observed in macaques (Supplementary Fig. 6f), indicating that H2 cells were more sensitive to aging processes in humans than in macaques. We also used immunostaining to verify the changes in HC cell type with aging. The number of H2-type cells decreased in both regions, whereas H1-type cells showed no change (Fig. 6g and h). By comparing the DEGs of H1 and H2 HCs, we found that HSP90AA1 and HSP90AB1, two heat shock proteins, were highly expressed in H1 but not H2 (Fig. 6i). These proteins can mediate lysosomes to refold unfolded proteins, thus protecting cells from the effects of protein toxicity [35]. This may be a reason why the H1 cells showed higher anti-aging ability than H2 cells.

For cones, the regional expression and localization of CALBINDIN showed no differences with aging. However, the subcellular localization of cone OPSINs changed from the outer segments to cell bodies in aged cones (both L/M and S cones) (Fig. 6j–m). It is possible that dysfunction of protein transportation in cilia leads to this mistrafficking and accumulation of cone opsins [36].

Human retinal disease related to gene expression in retinal cells

We used our scRNA-seq dataset to investigate the cell-type and region specificity of 178 genes associated with 55 types of human retinal disease, including night blindness, macula dystrophy, rod-cone dystrophy, dominant RP, recessive RP, AMD and recessive achromatopsia (RETNET, https://sph.uth.edu/retnet/). We first calculated the expression of each gene in the foveal or peripheral cell clusters and then aggregated the expression scores by disease types (Fig. 7a and b, Supplementary Fig. 7a and b). Generally, rods and cones, especially foveal cones, were highly related to night blindness and macula dystrophy (Fig. 7a and b). Genes related to rod-cone dystrophy, and dominant and recessive RP were highly expressed in rods and cones, particularly foveal photoreceptors in both humans and macaques. Genes related to AMD were highly enriched in foveal MG and cones, suggesting a correlation of regional cell subtype with this disease.

We further illustrated cell-type and region specificity of each gene categorized by disease. As expected, age-related degeneration AMD-risk genes were highly expressed in aged human retina but not in that of aged macaques (Fig. 7c and d), suggesting fewer aging characteristics in the macaque retina. Cell-type and region specificity of disease-related genes were further compared between humans and macaques (Fig. 7e and f, Supplementary Fig. 7a and b). For example, *PDE6A* and *PDE6B*, which are reported to cause recessive RP, were conservatively expressed in the rods in both primates (Fig. 7e and f). *HTRA1* which is a risk factor for AMD, were highly expressed in HCs in both humans and macaques but with differential regional preference (Fig. 7e and f). Another recessive RP-associated gene, *MVK* (mevalonate kinase), was enriched specifically in human peripheral HCs (Fig. 7e and f). Mutations of *EFEMP1* can lead to macular dystrophy [37], and the expression of *EFEMP1* was high in human and macaque foveal MGs (Fig. 7e and f). In addition, *ATF6*, a recessive achromatopsia-associated gene [38], was selectively expressed in human GCs located in the periphery, but showed no obvious expression in macaques (Fig. 7e and f). Together, these datasets showing region- and cell-type-specific expression patterns of retinal-disease-related genes should be useful for mechanistic and therapeutic studies of retinal diseases in the future.

DISCUSSION

By profiling 119,520 single cells, we provided detailed single-cell transcriptomes of adult and aged primate retinae with regional information. The retinal transcriptome at single-cell or single-nuclei level

has been reported [3,7–12]. In comparison with other single cell retina studies, we have the largest number of primate retinal samples in one study (six human samples and five macaque samples) covering the longest life span (8 days after birth to 87 years old for humans; 2–23 years old for macaques) so far. The non-human primate we used here is *Macaca mulatta*, which is evolutionarily closer to humans than *Macaca fascicularis* [3], adding more primate retinal transcriptome data to the retinal resource. Moreover, we did cross-species analysis between humans and macaques, and found the species-specific signatures of primate retinae, which provided valuable data sources to understand the regional and species specializations of the human and macaque retina. In particular, the study provided conceptual advances in the molecular characteristics of aging progress of human retina. Our data revealed that human retinal aging occurred in a region- and cell-type-specific manner, suggesting strong cell heterogeneity in retinal aging. Moreover, a big dataset was generated and showed the cell-type-, region-, and species-specific gene expression associated with various human retinal diseases, which provides a foundation to understanding of the molecular and cellular mechanisms underlying human retinal diseases. Overall, this study provides a valuable resource at the single-cell resolution to help understand human and macaque retina and related aging processes, study the regulatory mechanism of the aging process of human retina, and identify the molecular markers for aging and degenerative changes of human retina.

Different rod subtypes in human and macaque retina

We examined retinal cell-type evolutionary conservation between humans and macaques. The major cell types were conserved in the two species, but the molecular features in retinal cells showed species differences (Fig. 1f–k). Based on the expression level of *MYO9A*, the rods in humans and macaques can be divided into two groups. Our data indicated that the *MYO9A*$^{-}$ rod subtype was reduced during aging (Fig. 5i and j), which may result from either depletion of *MYO9A*$^{-}$ rods or increased *MYO9A*$^{+}$ cells. Considering that the proportion of *MYO9A*$^{-}$ cells was much more dramatically reduced in aged human retina than was the *MYO9A*$^{+}$ cells (Fig. 5i, Supplementary Fig. 5k), it is highly possible that the reduction of rods was largely a result of depletion of *MYO9A*$^{-}$ rods. Future studies are needed to investigate the functional role of *MYO9A* in rod photoreceptors. It is worth noting that we identified previously unidentified cell types. Cells in Cluster 46 of rod identity and Cluster 51 of MG identity co-expressed *OTX2* and *RLBP1* (Fig. 1d and e, Supplementary Fig. 1e). *OTX2* is a typical marker for BCs and rods, and *RLBP1* is a marker for MGs. MGs are considered to be retinal precursor cells in non-mammalian vertebrates and are able to transdifferentiate into rods and BCs with additional transcriptional and epigenetic regulation in mice [39,40]. The co-expression of *OTX2* and *RLBP1* suggests that MGs in Cluster 51 may be transcriptionally closer to rods and BCs. However, their function and potential to transdifferentiate into neuronal cells, such as rods or BCs, need further exploration.

Distinct transcriptomes of primate foveal and peripheral retina

With enriched cones, the fovea is the most important region for high-acuity vision in humans, whereas the peripheral retina helps direct eye movements to focus salient images on the fovea [41]. Based on their different functions, they showed distinct molecular signatures in MGs and cones (Fig. 3a, b, h and i). Several genes were found to be specifically enriched in foveal MGs, for example *RGR*, *HTR1*, *DIO2* and *CYP26A1*. The finding of specific high *RGR* expression in foveal MGs is interesting. *RGR* is a non-visual opsin in intracellular membranes of RPE and MGs. Previous study suggests that RGR opsin and retinol dehydrogenase-10 (*Rdh10*) convert all-trans-retinol to 11-cis-retinol for the regeneration of cone visual pigment in daylight, as RPE cannot meet the higher needs of the visual opsins in rods and cones in daylight [28]. An intriguing speculation is that the higher expression of *RGR* in fovea MGs is initiated to meet the higher demands of visual pigment regeneration in foveal cones.

In addition to *RGR* and retinol, we also found that MGs and cones possibly interact with each other via the TH signaling pathway. As the active form of TH, T3 is important for cone development in retina and retinal organoids [33,42]. However, it remains unclear whether TH signals exhibit regionally specific distribution in primate retina, and which cell types may provide TH. The major TH in blood is inactive T4, which needs to be converted to T3 by DIO2. Interestingly, we found *DIO2* to be selectively expressed in foveal MGs. Accordingly, we found that cone photoreceptors expressed *THRβ*, a nuclear receptor of T3. Based on our ATAC-seq data, we observed the binding sites of *THRβ* in the promoter regions of *RFC1*, *APLP2* and *POLE4*, which are genes specifically expressed in foveal cones. Hence, it is possible that the expression of *DIO2* in foveal MGs may produce high local T3, which modulates the expression of a specific set of

genes in foveal cones. Of note, higher expression of *NPVF*, which is negatively regulated by the TH signaling pathway [43], was detected in the peripheral cones and MGs. Together, our data imply that foveal MGs may provide a local TH signal that regulates the cellular specificity of foveal and peripheral cones.

Cellular and molecular changes accompanying human retinal aging

Our study explored cellular and molecular changes during primate retina aging. GO term analysis revealed that microglial cell activation, protein refolding, oxygen species metabolism and cell death were highly enriched in aging retina and could possibly be considered as hallmarks for retinal aging. In healthy retinae, microglial cells are innate immune cells, which can constantly adapt to their microenvironment. In mouse models, increased density and activation of microglia exist in aged retinae and brains, as well as in age-related human diseases, including AMD, Alzheimer's disease (AD) and Parkinson's disease (PD) [44,45]. Similarly, the human retina showed an increased number of microglia during aging (Fig. 5h). Moreover, microglial activation and microglia-mediated inflammatory responses can generate a chronic mild inflammatory environment, including an increased production of inflammatory cytokines, reactive oxygen species (ROS) and reactive nitrogen species (RNS) [46], which can further accelerate retinal aging and pathogenesis of age-related diseases. Thus, we speculated that targeting microglial activation states could potentially be used as a therapeutic avenue in slowing aging and retinal diseases.

Mistrafficking and accumulation of both rod and cone opsins (Fig. 5g and Fig. 6j and l) were found in the aging retina. Damaged protein accumulation can lead to toxicity against photoreceptors as these failed homeostatic mechanisms can contribute to pathology [36]. Therefore, protein misfolding may be a causative reason for apoptosis of photoreceptors during aging. Other than protein misfolding, retinal oxygen supply also decreases with age. Thus, aging retinae suffer from low-grade chronic ischemia [47], which can lead to retinal oxidative stress in turn. MGs in the peripheral retina exhibited high expression of metallothioneins (*MT3*, *MT1G* and *MT2A*) and glutathione peroxidase 3 (*GPX3*), which participate in an array of protective stress responses [48]. Metallothioneins are a family of cysteine-rich metal-binding proteins involved in protection against oxidative stress and buffering against toxic heavy metals [49]. As a major scavenger of ROS in plasma, *GPX3* acts as a redox signal modulator [50]. The high levels of metallothioneins and *GPX3* in the peripheral MGs may contribute to fovea to peripheral aging gradient observed in human retina.

VEGF is a well-known risk factor for abnormal retinal angiogenesis in AMD and diabetic retinopathy. We found that VEGF-A expression increased specifically in HCs, MGs and astrocytes following aging. VEGF is a potent endothelial cell mitogen that stimulates proliferation, migration and tube formation, leading to angiogenic growth of blood vessels [51]. With the knowledge that cellular origin of VEGF-A increases during aging, it is possible to design therapeutic approaches to reduce its expression in MGs, HCs and astrocytes for abnormal retinal angiogenesis treatment. Other than VEGF, we observed several previously unidentified genes associated with aging, for example *NPVF*, *PCP4*, *CRYAA* and *B2M*. Altogether, our study provides a valuable data source for future studies on human retinal aging and related diseases.

Cell-type and region specificity of human retinal diseases

Our study provides a foundation to understand the molecular and cellular mechanisms underlying human retinal diseases. By assessing the expression of 178 genes implicated in human retinal diseases, we found that these genes were preferentially expressed in specific retinal cell classes and regions. Photoreceptors in foveal regions are the major cell types for many retinal degenerative diseases. These findings emphasized the value of human aging transcriptomes for age-related retinal diseases. In particular, AMD-risk genes were highly expressed in the aged human retina. Together, the region- and cell-type-specific expression patterns of retinal disease-related genes may provide guidelines for future cellular and molecular precision therapies.

MATERIALS AND METHODS

Human retinal samples

The isolation procedure of human retinal samples and research protocols were approved by the Research Ethics committee of the Peking University Third Hospital and Peking Union Medical College Hospital, and were conducted in accordance with approved institutional guidelines. All the protocols are in compliance with the 'Interim Measures for the Administration of Human Genetic Resources,' administered by the Ministry of Science and Technology of China.

Macaque retinal samples

Rhesus macaques (*Macaca mulatta*) were provided by Xieerxin Biology Resource (Beijing, China). All procedures were conducted in accordance with the Principles for the Ethical Treatment of Non-Human Primates and were approved by the Institutional Animal Care and Use Committee of the Institute of Biophysics and University of Science and Technology of China. All animals were maintained at 25°C on a 12 hour light:12 hour dark schedule at Xieerxin Biology Resource, a Laboratory Animal Care-accredited facility in Beijing, in compliance with all local and federal laws governing animal research. Animals were given a commercial diet twice a day with tap water provided *ad libitum* and were fed vegetables and fruits once daily under careful veterinary oversight. Before the experiment, none of the animals had a clinical or experimental history that would affect physiological aging or increase disease susceptibility.

Statistical analyses

All data were represented as means ± s.e.m. Comparisons between two groups were made using *t*-tests. Quantification graphs were analyzed using GraphPad Prism (GraphPad Software).

DATA AND CODE AVAILABILITY

The single-cell RNA-seq and bulk ATAC-seq data used in this study were all deposited in the Genome Sequence Archive (GSA) for Human, National Genomics Data Center (https://bigd.big.ac.cn/gsa-human) under BioProject accession numbers PRJCA002731. The GSA number for macaque is CRA002680 and the GSA number for Human is HRA000182. All codes for data analysis are included in Supplementary file 1.

SUPPLEMENTARY DATA

Supplementary data are available at *NSR* online.

ACKNOWLEDGEMENTS

We thank the National Human Brain Bank for Development of Function. We thank Dr. Kun Qu (University of Science and Technology of China) for data analysis advice.

FUNDING

This work was supported by the National Key Research and Development Program of China (2020YFA0112200), the Strategic Priority Research Program of the Chinese Academy of Sciences (XDA16020601/03 and XDB39000000), the National Key Research and Development Program of China (2019YFA0110100, 2017YFA0103303 and 2017YFA0102601), the National Natural Science Foundation of China (81925009, 81790644, 31671072, 81891001, 81900855, 31771140 and 31900712), the Fundamental Research Funds for the Central Universities (WK2070000174 and WK2090050048), the National Resource Center for Non-Human Primates and Beijing Brain Initiative of Beijing Municipal Science & Technology Commission (Z181100001518004).

AUTHOR CONTRIBUTIONS

T.X., X.W., Q.W. and M.Z. conceived the project and designed the experiments. W.Y., S.Z., M.W., H.X. and M.Z. performed RNA-seq. Y.L., H.D. and M.W. analyzed the data. W.Y. and Q.W. performed immunofluorescence and imaging. W.Y. and H.X. prepared the ATAC-seq library. W.Y. and Y.L. performed RNAscope ISH. Z.Y., Y.T., H.Q., R.P., J.H., Y.M., S.L., W.W., Q.M., Z.L., C.Y., S.L., J.W. and C.M. prepared the primate samples. T.X., X.W., Q.W. and M.Z. wrote the manuscript with input from all other authors. All authors edited and proofread the manuscript.

Conflict of interest statement. None declared.

REFERENCES

1. Masland RH. The neuronal organization of the retina. *Neuron* 2012; **76**: 266–80.
2. Cepko CL. The determination of rod and cone photoreceptor fate. *Annu Rev Vis Sci* 2015; **1**: 211–34.
3. Peng YR, Shekhar K and Yan W *et al.* Molecular classification and comparative taxonomics of foveal and peripheral cells in primate retina. *Cell* 2019; **176**: 1222–37.
4. Cepko C. Intrinsically different retinal progenitor cells produce specific types of progeny. *Nat Rev Neurosci* 2014; **15**: 615–27.
5. Hoshino A, Ratnapriya R and Brooks MJ *et al.* Molecular anatomy of the developing human retina. *Dev Cell* 2017; **43**: 763–79.
6. Franze K, Grosche J and Skatchkov SN *et al.* Muller cells are living optical fibers in the vertebrate retina. *Proc Natl Acad Sci USA* 2007; **104**: 8287–92.
7. Liang Q, Dharmat R and Owen L *et al.* Single-nuclei RNA-seq on human retinal tissue provides improved transcriptome profiling. *Nat Commun* 2019; **10**: 5743.
8. Lukowski SW, Lo CY and Sharov AA *et al.* A single-cell transcriptome atlas of the adult human retina. *EMBO J* 2019; **38**: e100811.
9. Menon M, Mohammadi S and Davila-Velderrain J *et al.* Single-cell transcriptomic atlas of the human retina identifies cell types associated with age-related macular degeneration. *Nat Commun* 2019; **10**: 4902.
10. Orozco LD, Chen H-H and Cox C *et al.* Integration of eQTL and a Single-Cell atlas in the human eye identifies causal genes for Age-Related Macular Degeneration. *Cell Rep* 2020; **30**: 1246–59.
11. Sridhar A, Hoshino A and Finkbeiner CR *et al.* Single-Cell transcriptomic comparison of human fetal retina, hPSC-Derived retinal organoids, and long-term retinal cultures. *Cell Rep* 2020; **30**: 1644–59.
12. Voigt AP, Whitmore SS and Flamme-Wiese MJ *et al.* Molecular characterization of foveal versus peripheral human retina by single-cell RNA sequencing. *Exp Eye Res* 2019; **184**: 234–42.
13. Owsley C. Aging and vision. *Vision Res* 2011; **51**: 1610–22.

14. Moshiri A, Chen R and Kim S *et al.* A nonhuman primate model of inherited retinal disease. *J Clin Invest* 2019; **129**: 863–74.
15. Newsome WT and Stein-Aviles JA. Nonhuman primate models of visually based cognition. *ILAR J* 1999; **39**: 78–91.
16. Hendrickson A. A morphological comparison of foveal development in man and monkey. *Eye (Lond)* 1992; **6**: 136–44.
17. Roorda A, Metha AB and Lennie P *et al.* Packing arrangement of the three cone classes in primate retina. *Vision Res* 2001; **41**: 1291–306.
18. Ximerakis M, Lipnick SL and Innes BT *et al.* Single-cell transcriptomic profiling of the aging mouse brain. *Nat Neurosci* 2019; **22**: 1696–708.
19. Hendrickson A, Bumsted-O'Brien K and Natoli R *et al.* Rod photoreceptor differentiation in fetal and infant human retina. *Exp Eye Res* 2008; **87**: 415–26.
20. Vazquez-Chona FR, Clark AM and Levine EM. Rlbp1 promoter drives robust Muller glial GFP expression in transgenic mice. *Invest Ophthalmol Vis Sci* 2009; **50**: 3996–4003.
21. Welch JD, Kozareva V and Ferreira A *et al.* Single-Cell multi-omic integration compares and contrasts features of brain cell identity. *Cell* 2019; **177**: 1873–87.
22. Clark BS, Stein-O'Brien GL and Shiau F *et al.* Single-Cell RNA-Seq analysis of retinal development identifies NFI factors as regulating mitotic exit and late-born cell specification. *Neuron* 2019; **102**: 1111–26.
23. Zhu X, Wu K and Rife L *et al.* Carboxypeptidase E is required for normal synaptic transmission from photoreceptors to the inner retina. *J Neurochem* 2005; **95**: 1351–62.
24. Farioli-Vecchioli S, Micheli L and Saraulli D *et al.* Btg1 is required to maintain the pool of stem and progenitor cells of the dentate gyrus and subventricular zone. *Front Neurosci* 2012; **6**: 124.
25. Lu Y, Shiau F and Yi W *et al.* Single-Cell analysis of human retina identifies evolutionarily conserved and species-specific mechanisms controlling development. *Dev Cell* 2020; **53**: 473–91.
26. da Silva S and Cepko CL. Fgf8 expression and degradation of retinoic acid are required for patterning a high-acuity area in the retina. *Dev Cell* 2017; **42**: 68–81.
27. Tufford A and Cayouette M. RA gets out of the way to allow high-acuity vision. *Dev Cell* 2017; **42**: 3–5.
28. Morshedian A, Kaylor JJ and Ng SY *et al.* Light-Driven regeneration of cone visual pigments through a mechanism involving RGR opsin in muller glial cells. *Neuron* 2019; **102**: 1172–83.
29. Wang JS and Kefalov VJ. The cone-specific visual cycle. *Prog Retin Eye Res* 2011; **30**: 115–28.
30. Lin MK, Yang J and Hsu CW *et al.* HTRA1, an age-related macular degeneration protease, processes extracellular matrix proteins EFEMP1 and TSP1. *Aging Cell* 2018; **17**: e12710.
31. Bringmann A, Syrbe S and Görner K *et al.* The primate fovea: structure, function and development. *Prog Retin Eye Res* 2018; **66**: 49–84.
32. Arrojo EDR, Fonseca TL and Werneck-de-Castro JPS *et al.* Role of the type 2 iodothyronine deiodinase (D2) in the control of thyroid hormone signaling. *Biochim Biophys Acta* 2013; **1830**: 3956–64.
33. Eldred KC, Hadyniak SE and Hussey KA *et al.* Thyroid hormone signaling specifies cone subtypes in human retinal organoids. *Science* 2018; **362**: eaau6348.
34. Nowakowski TJ, Bhaduri A and Pollen AA *et al.* Spatiotemporal gene expression trajectories reveal developmental hierarchies of the human cortex. *Science* 2017; **358**: 1318–23.
35. Penke B, Bogár F and Crul T *et al.* Heat shock proteins and autophagy pathways in neuroprotection: from molecular bases to pharmacological interventions. *Int J Mol Sci* 2018; **19**: 325.
36. Zhang T, Zhang N and Baehr W *et al.* Cone opsin determines the time course of cone photoreceptor degeneration in Leber congenital amaurosis. *Proc Natl Acad Sci USA* 2011; **108**: 8879–84.
37. Thompson S, Blodi FR and Larson DR *et al.* The Efemp1^{R345W} macular dystrophy mutation causes amplified circadian and photophobic responses to light in mice. *Invest Ophthalmol Vis Sci* 2019; **60**: 2110–7.
38. Ansar M, Santos-Cortez RLP and Saqib MAN *et al.* Mutation of ATF6 causes autosomal recessive achromatopsia. *Hum Genet* 2015; **134**: 941–50.
39. Jorstad NL, Wilken MS and Grimes WN *et al.* Stimulation of functional neuronal regeneration from Muller glia in adult mice. *Nature* 2017; **548**: 103–7.
40. Yao K, Qiu S and Wang YV *et al.* Restoration of vision after de novo genesis of rod photoreceptors in mammalian retinas. *Nature* 2018; **560**: 484–8.
41. Marfil R, Palomino AJ and Bandera A. Combining segmentation and attention: a new foveal attention model. *Front Comput Neurosci* 2014; **8**: 96.
42. Glaschke A, Weiland J and Del Turco D *et al.* Thyroid hormone controls cone opsin expression in the retina of adult rodents. *J Neurosci* 2011; **31**: 4844–51.
43. Son YL, Ubuka T and Tsutsui K. Molecular Mechanisms of gonadotropin-inhibitory hormone (GnIH) actions in target cells and regulation of GnIH expression. *Front Endocrinol (Lausanne)* 2019; **10**: 110.
44. Henry V, Paillé V and Lelan F *et al.* Kinetics of microglial activation and degeneration of dopamine-containing neurons in a rat model of Parkinson disease induced by 6-hydroxydopamine. *J Neuropathol Exp Neurol* 2009; **68**: 1092–102.
45. Indaram M, Ma W and Zhao L *et al.* 7-Ketocholesterol increases retinal microglial migration, activation, and angiogenicity: a potential pathogenic mechanism underlying age-related macular degeneration. *Sci Rep* 2015; **5**: 9144.
46. von Bernhardi R, Eugenin-von Bernhardi L and Eugenin J. Microglial cell dysregulation in brain aging and neurodegeneration. *Front Aging Neurosci* 2015; **7**: 124.
47. Chen M, Luo C and Zhao J *et al.* Immune regulation in the aging retina. *Prog Retin Eye Res* 2019; **69**: 159–72.
48. Ruttkay-Nedecky B, Nejdl L and Gumulec J *et al.* The role of metallothionein in oxidative stress. *Int J Mol Sci* 2013; **14**: 6044–66.
49. Guo R, Ma H and Gao F *et al.* Metallothionein alleviates oxidative stress-induced endoplasmic reticulum stress and myocardial dysfunction. *J Mol Cell Cardiol* 2009; **47**: 228–37.
50. Delaunay A, Pflieger D and Barrault MB *et al.* A thiol peroxidase is an H_2O_2 receptor and redox-transducer in gene activation. *Cell* 2002; **111**: 471–81.
51. Niu G and Chen X. Vascular endothelial growth factor as an anti-angiogenic target for cancer therapy. *Curr Drug Targets* 2010; **11**: 1000–17.